

Effect of Deformation-Induced Martensite on Protective Performance of Passive Film on 304 Stainless Steel

Shanlin He^{1,*}, Daming Jiang¹, Zhaoyuan Sun²

¹ School of Materials Science and Engineering, Harbin Institute of Technology, Harbin 150001, China

² Center of Analysis and Measurement, Harbin Institute of Technology, Harbin 150001, China

*E-mail: 11B909025@hit.edu.cn

Received: 15 January 2018 / *Accepted:* 26 February 2018 / *Published:* 10 April 2018

The relationships among the characteristics and electrochemical properties of passive films on the surfaces of 304 stainless steel specimens with different deformation-induced martensite content were examined using X-ray diffraction spectroscopy (XRD), transmission electron microscopy (TEM), X-ray photoelectron spectroscopy (XPS) and electrochemical methods. The compound contents and protective performance of the passive film initially decreased and then increased with increasing deformation-induced martensite content. The passive film on the surface of a stainless steel specimen with an α' -martensite content of 6% was found to have the lowest contents of compounds and the poorest protective performance. When the α' -martensite content was less than 6%, the compound contents and protective performance of the passive film on the surface of the stainless steel decreased with increasing α' -martensite content. When the α' -martensite content exceeded 6%, the compound contents and protective performance of the passive film increased to a certain extent with increasing α' -martensite content.

Keywords: martensite; passive film; 304 stainless steel; protective performance

1. INTRODUCTION

Due to its exceptional corrosion resistance and mechanical and welding properties, 304 stainless steel is extensively used in industrial production[1-8]. For an austenitic stainless steel, its corrosion resistance is significantly affected by the deformation-induced martensite inside it and the passive film on its surface[9-16]. In the as-supplied state, the structure of 304 stainless steel consists almost of the pure austenite, and a passive film with a thickness of approximately 10 nm is formed on its surface after acid pickling and passivation[13,16,17]. In addition, 304 stainless steel has a metastable austenitic structure. Cold working can cause some of the austenite inside 304 stainless steel to transform to α' -martensite and ϵ -martensite and damage the original surface film to varying degrees[9,12,14,17-19]. Measurements have shown that deformation-induced martensite with a

volume fraction of approximately 20% formed in the areas of corrugated pipes with various specifications where significant deformation occurred during the working process. Martensite can significantly reduce the corrosion resistance of austenitic stainless steels and can easily induce stress corrosion damage, which can cause catastrophic incidents[20-24]. Relevant research has noted that deformation-induced martensite phase transformations are among the main causes of stress corrosion cracking in austenitic stainless steels in chloride ion containing solution media[25]. An increase in plastic deformation will lead to an increase in the α' -martensite content, thereby causing the material structure to undergo significant changes[26]. The donor and acceptor densities of passive films increase almost linearly with the α' -martensite content[9]. It is well known that the passive film on the surface of 304 stainless steel can naturally recover in oxidation environments such as air, nitric acid and solutions containing dissolved oxygen[27-30]. However, the performance of the passive film, as well as its stability in solutions, will change significantly after plastic deformation[12,14,31,32].

Although the protective performance of passive films has been studied under various strain rates, the deformation-induced martensite content significantly differs under the same strain rate due to the effects of tensile strength or temperature[12,14,18,21-23,31]. The protective performance of passive films on the surfaces of materials containing deformation-induced martensite has been infrequently studied[32]. Thus, further research is needed to understand the effects of deformation-induced martensite on the performance of the passive film on 304 stainless steel.

2. EXPERIMENTAL

2.1 Material and specimen preparation

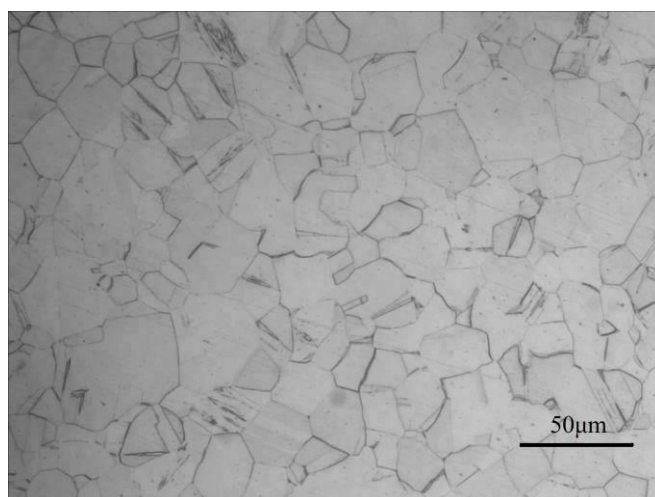


Figure 1. Microscopic image of the 304 stainless steel after solution treatment (heated to 1,050 °C for 30 min and cooled to room temperature in air) at a magnitude of 500X.

A 3-mm-thick commercial grade 304 stainless steel plate was selected as the experimental material. The chemical composition of the stainless steel plate is as follows: carbon (C): 0.04%; silicon (Si): 0.55%; manganese (Mn): 1.28%; chromium (Cr): 18.2%; nickel: 8.02%; and iron (Fe): 71.91%.

The stainless steel plate was first subjected to a solution treatment: it was heated to 1,050 °C and maintained at this temperature for 30 min, after which it was allowed to cool in air to room temperature. Figure 1 shows the microscopic image of the material structure after the solution treatment, it can be seen that after the solution treatment, the matrix of the 304 stainless steel consisted of uniformly distributed equiaxed austenite grains with distinct and regular grain boundaries.

The solution treated stainless steel plate was soaked in a 5 °C water bath and rapidly cold rolled. By controlling the amounts of compression at the level of 1%, 8%, 14% and 23% during the cold rolling process, specimens with martensite contents of 0.6%, 6%, 12% and 20% were prepared. The martensite content was measured using a ferrite content measuring instrument (FISCHER, FERITSCOPE MP30E-S), the specimen was cleaned in acetone solution, blow-dried in air and then placed on a flat glass plate before the measurement, the probe of the measuring instrument was fixed above the test area of the specimen, and the ferrite content was obtained after the reading reached steady state, each specimen was measured at least three times in order to ensure the data accuracy.

2.2. Electrochemical test

To understand the changes in the protective performance of the passive films on the surfaces of different microstructures, each specimen was analyzed based on polarization and impedance measurements. The preprocessing procedure is as follows. A $\phi 15$ -mm circular test piece was cut from each specimen and then polished in water using metallographic sandpaper and subsequently rinsed with acetone and ethyl alcohol. Afterward, each test piece was soaked in a 90 °C deionized water bath for 24 h to allow a stable passive film to form on its surface. Then, each test piece was tested to determine its electrochemical impedance spectroscopy (EIS) spectrum and polarization curve on an REF 3000 electrochemical workstation (Gamry). A three-electrode system (anode: graphite; reference electrode: silver chloride; and working electrode: test piece) was used for the measurements. A 3.5% sodium chloride (NaCl) solution at 90 °C was used as the test medium. The potential was scanned from -0.2 to 2 V at a rate of 0.5 mV/s.

2.3. X-ray photoelectron spectroscopy (XPS) analysis of the surface films

XPS was used to analyze the composition of the passive film on the surface of each specimen. The XPS specimens were prepared in the same way as the electrochemical test specimens. A 4-mm \times 6-mm rectangular test piece was cut from each prepared specimen, which was rinsed with acetone and ethyl alcohol and then blow dried and subsequently subjected to XPS analysis.

2.4. Material structure analysis

The microstructures were analyzed using optical microscopy, X-ray diffraction spectroscopy (XRD) and transmission electron microscopy (TEM). The optical microscopy and XRD specimens were prepared using the same method. A $\phi 10$ -mm circular test piece was cut from each specimen.

Each piece was polished using metallographic sandpaper and subsequently corroded in a 10% oxalic acid solution for 10 s. Next, each test piece was subjected to an optical microscopic examination using an Olympus PMG2 optical microscope and XRD analysis using a Rigaku Ultimal IV diffractometer with filtered $\text{CuK}\alpha$ radiation ($\lambda=0.154056$ nm).

A $\phi 10$ -mm circular test piece was cut from each specimen for TEM analysis. Each test piece was slowly polished using metallographic sandpaper in water until a thickness of approximately $50\ \mu\text{m}$ was reached. Afterward, each test piece was thinned using a twin-jet electropolisher at a voltage of 32 V and a temperature varying from $-10\ ^\circ\text{C}$ to $-5\ ^\circ\text{C}$. TEM analysis was performed with a Tecnai G220 transmission electron microscope at an acceleration voltage of 200 kV.

3. RESULTS

3.1 Changes in the material structure

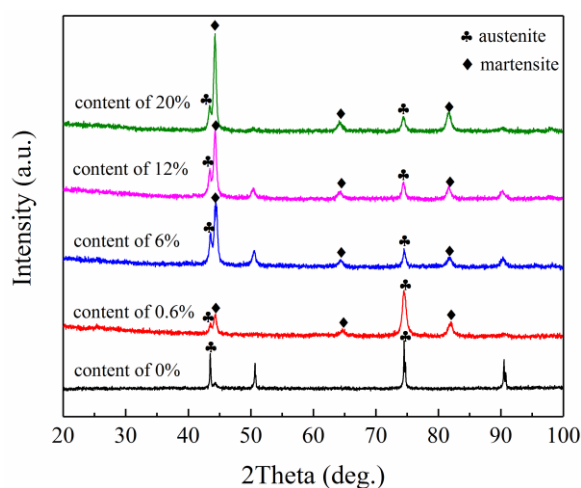
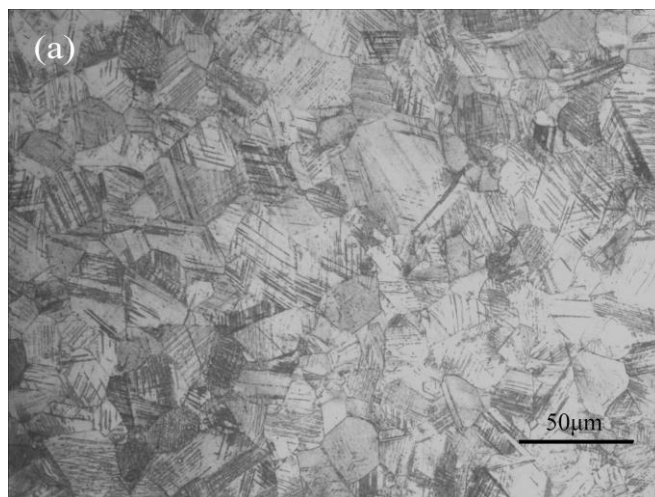


Figure 2. XRD patterns of the 304 stainless steel specimens with various martensite contents before and after cold rolling.



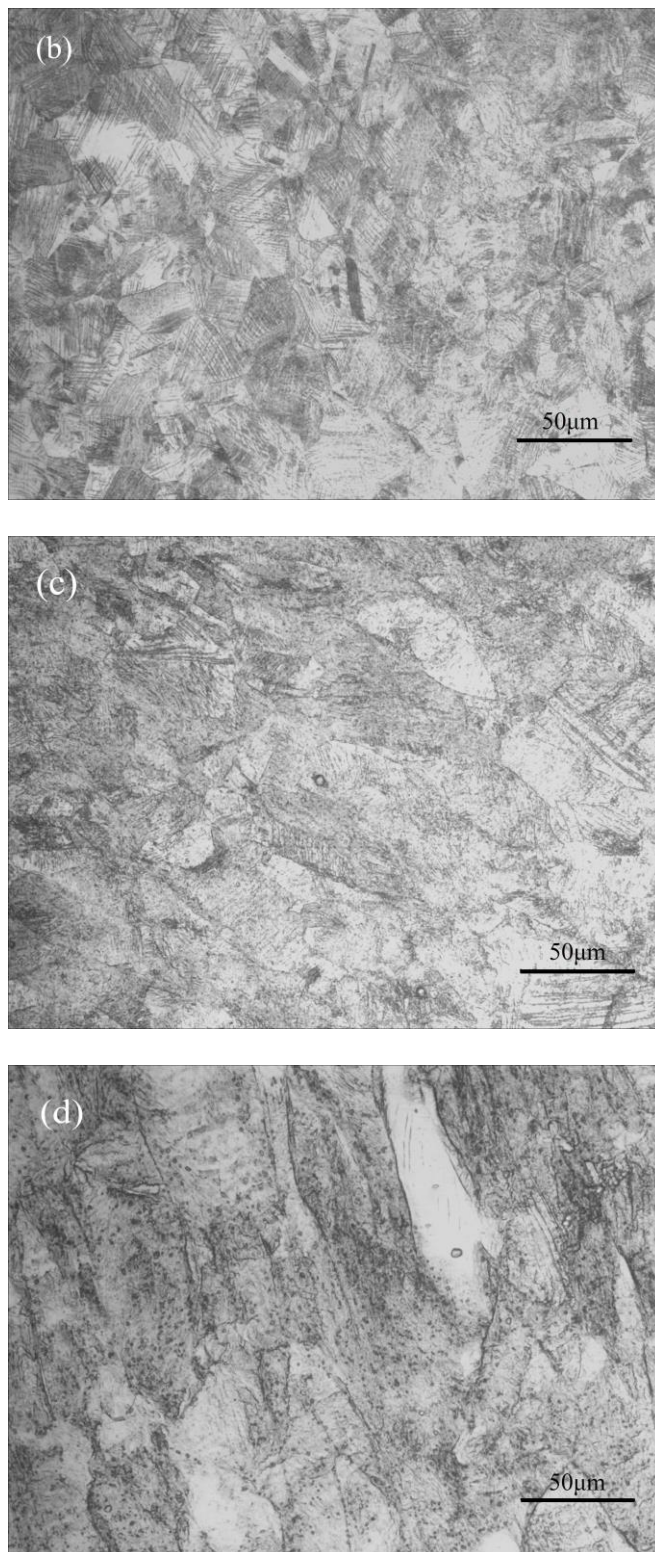
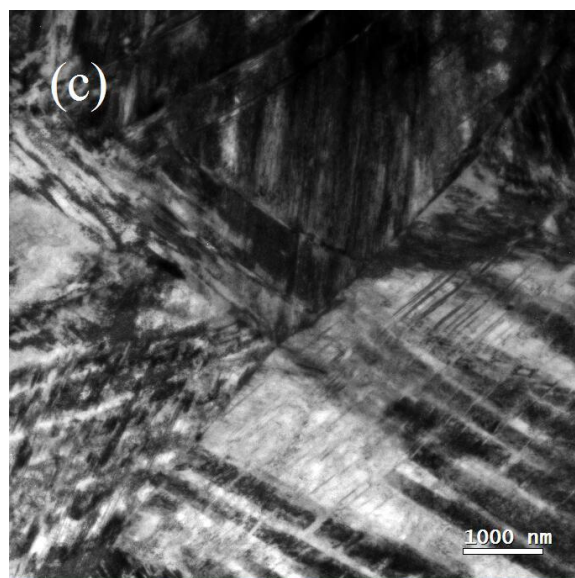
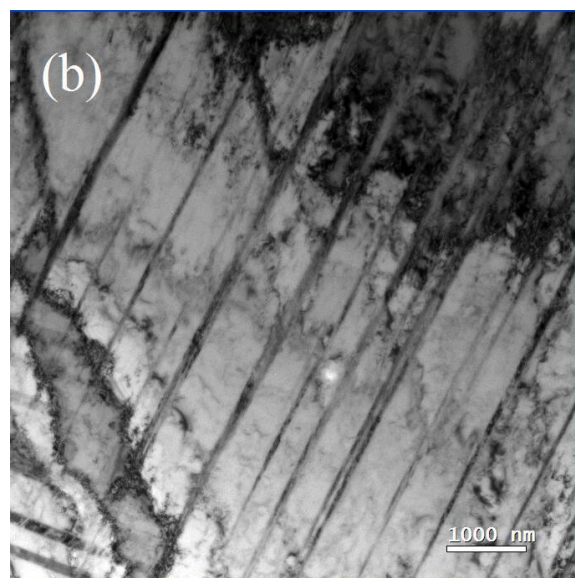
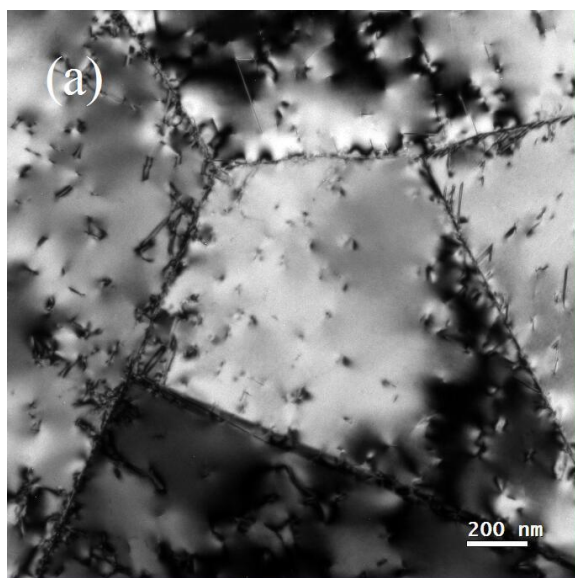


Figure 3. Microscopic images of the 304 stainless steel specimens with various martensite contents after cold rolling at a magnitude of 500X: (a) specimen with an α' -martensite content of 0.6%; (b) specimen with an α' -martensite content of 6%; (c) specimen with an α' -martensite content of 12% and (d) specimen with an α' -martensite content of 20%.



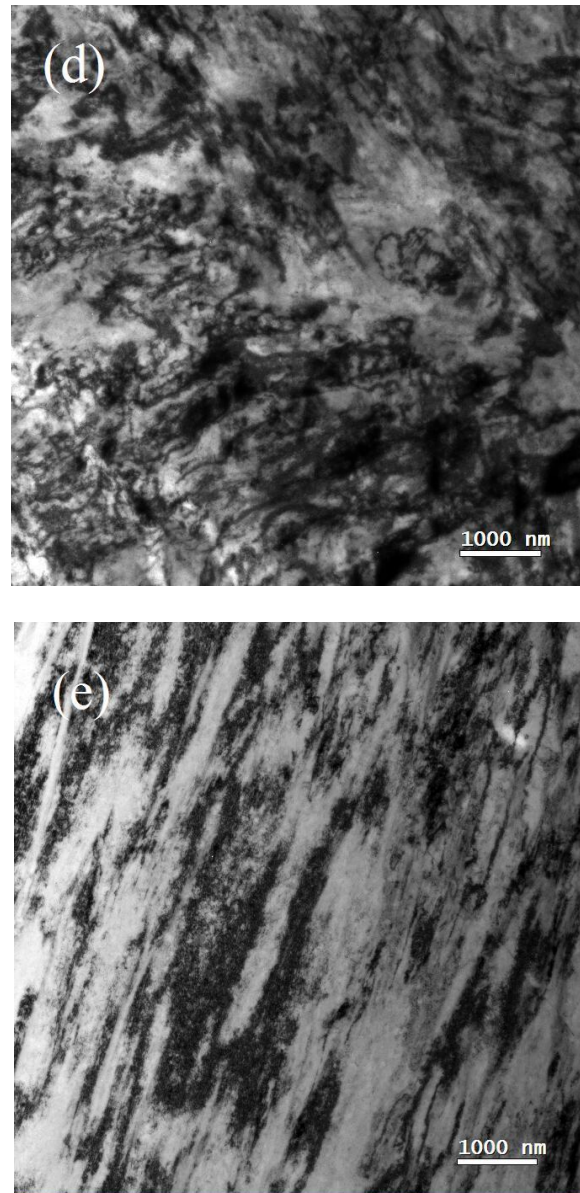


Figure 4. TEM images of the 304 stainless steel specimens with various martensite contents before and after cold rolling: (a) specimen with an α' -martensite content of 0%; (b) specimen with an α' -martensite content of 0.6%; (c) specimen with an α' -martensite content of 6%; (d) specimen with an α' -martensite content of 12% and (e) specimen with an α' -martensite content of 20%.

Figure 2 shows the XRD patterns of the 304 stainless steel specimens with various martensite contents before and after cold rolling. Based on the characteristic peak locations, the $\gamma(111)$, $\gamma(311)$, $\gamma(220)$ and $\gamma(200)$ peaks were the main diffraction peaks of the test specimens after the solution treatment. After the cold rolling process, the intensities of the $\gamma(111)$ and $\gamma(220)$ diffraction peaks gradually decreased, whereas the $\gamma(311)$ and $\gamma(200)$ peaks almost disappeared.

After the occurrence of deformation, the $\alpha'(110)$, $\alpha'(211)$ and $\alpha'(200)$ peaks became the new diffraction peaks. In terms of peak intensity, the intensity of the $\alpha'(110)$ peak rapidly increased with increasing martensite content.

Figure 3 shows microscopic images of the 304 stainless steel specimens with various martensite contents after cold rolling. As the α' -martensite content reached 0.6%, the grains underwent slight deformation, with lath martensite appearing inside them. When the α' -martensite content reached 6%, the grains underwent substantial deformation, and the lath martensite density inside the grains significantly increased. When the α' -martensite content reached 12%, the grain boundaries considerably extended in the direction of plastic deformation, and the lath martensite became disorderly. When the α' -martensite content reached 20%, the grains underwent relatively significant deformation, and the initial grain morphology was no longer recognizable.

Figure 4 shows TEM images of the 304 stainless steel specimens with various martensite contents before and after cold rolling. After the solution treatment, the 304 stainless steel exhibited a uniform equiaxed austenitic structure with dislocations distributed inside the grains. When the α' -martensite content reached 0.6%, distinct and parallel long lath martensite appeared inside the grains. When the α' -martensite content reached 6%, crossed lath martensite appeared inside the grains. In addition, the number of defects in the material structure significantly increased, but the grain boundaries remained distinct. When the α' -martensite content reached 12%, the martensite exhibited a short lath shape, and a large number of disorderly dislocation tangles appeared inside the grains. When the α' -martensite content reached 20%, dislocation tangles distributed in a banded pattern in the direction of deformation were observed, and the original austenite grain boundaries were no longer recognizable.

3.2 Changes in the electrochemical properties

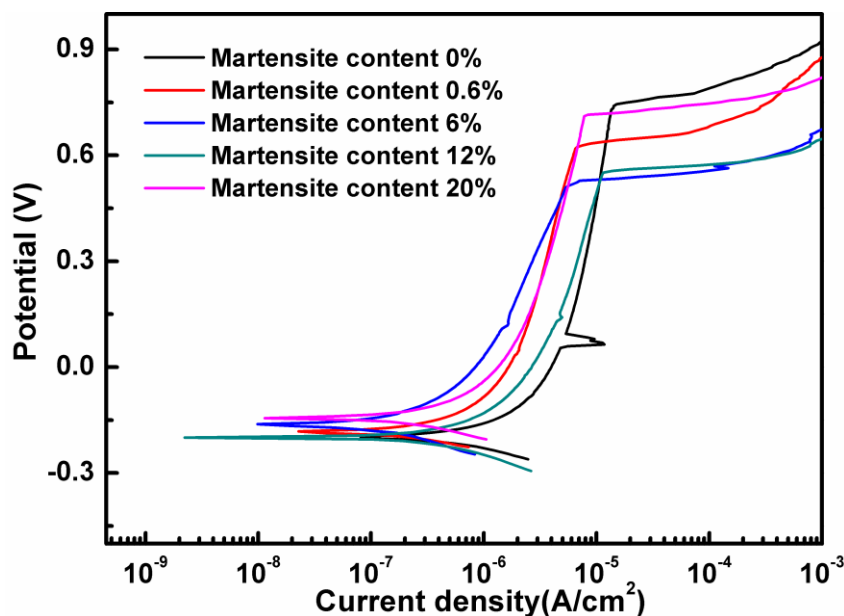


Figure 5. Polarization curves of the 304 stainless steel specimens with various martensite contents before and after cold rolling in a 3.5% sodium chloride (NaCl) solution at 90 °C.

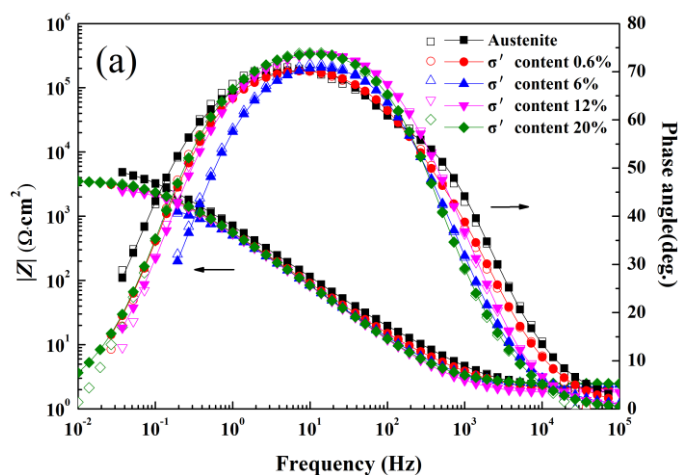
Figure 5 shows the polarization curves of the 304 stainless steel specimens with various martensite contents before and after cold rolling. Overall, the curve of each specimen has a clear

passivation region. Table 1 summarizes the corrosion parameters obtained from the polarization curves shown in Figure 5. From the table, it is clear that the breakdown potential of the specimen with an α' -martensite content of 6% was the lowest, indicating that this specimen had the lowest corrosion resistance. When the α' -martensite content was less than 6%, the corrosion resistance (breakdown potential) of the stainless steel decreased with increasing α' -martensite content. When the martensite content exceeded 6%, the corrosion resistance (breakdown potential) of the stainless steel increased to a certain extent with increasing α' -martensite content.

Table 1. Corroison parameters obtained from the polarization curves of the 304 stainless steel specimens with various martensite contents before and afer cold rolling in a 3.5% sodium chloride (NaCl) solution at 90 °C.

Martensite content (%)	Open circuit potential (mV)	Breakdown potential (mV)	Passivation current (A/cm ²)	Corroison current (A/cm ²)	Tafel slope anode (mV/dec)	Tafel slope cathode (mV/dec)
0	-200.5	739.4	1.42E-5	3.51E-6	1634.9	-491.1
0.6	-181.7	623.5	6.75E-6	1.27E-6	1198.4	-28.2
6	-161.3	508.8	5.32E-6	5.09E-7	716.4	-45.8
12	-199.1	551.1	1.14E-5	2.02E-6	1087.9	-34.5
20	-144.6	710.5	7.78E-6	1.47E-6	1229.9	-32.1

To thoroughly analyze the mechanism by which the protective performance of the passive film changed, the Bode plots and Nyquist plots of the 304 stainless steel specimens with various martensite contents before and afer cold rolling were derived from the EIS measurements (as shown in Figure 6). The results show that the radius of the semicircle of the Nyquist plot of the annealed austenite is the largest. The radius of the semicircle of the Nyquist plot decreases with increasing α' -martensite content when the α' -martensite content is in the range of <6%, reaches a minimum value when the α' -martensite content reaches 6% and starts to increase with increasing α' -martensite content when the α' -martensite content exceeds 6%.



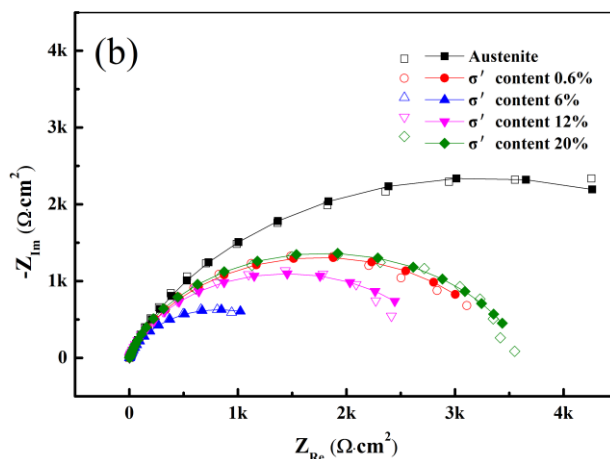


Figure 6. Bode plots and Nyquist plots of the 304 stainless steel specimens with various martensite contents before and after cold rolling in a 3.5% sodium chloride (NaCl) solution at 90 °C: (a) Bode plots and (b) Nyquist plots.

This result indicates that when the α' -martensite content was less than 6%, the protective performance of the passive film decreased with increasing α' -martensite content. When the α' -martensite content exceeded 6%, the protective performance of the passive film increased to some extent with increasing α' -martensite content. This finding is consistent with the observations based on from the polarization curves.

Figure 7 shows the equivalent circuit model used to fit the EIS data shown in Figure 6. In the model, R_s is the resistance of the electrolyte solution, R_m is the resistance of the passive film, R_{ct} is the resistance inside the pores of the passive film, Q_m is the constant phase element, and C_d is the double-layer capacitance.

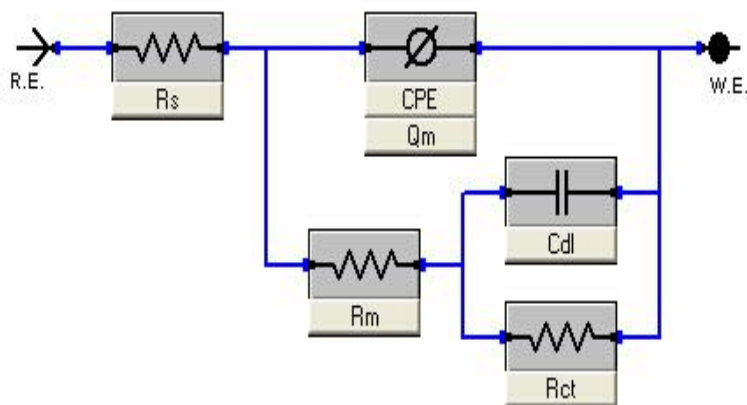


Figure 7. Equivalent circuit model used to fit the EIS data of the 304 stainless steel specimens with various martensite contents before and after cold rolling in a 3.5% sodium chloride (NaCl) solution at 90 °C.

Table 2. Electrochemical parameters fitted from the EIS data of the 304 stainless steel specimens with various martensite contents before and after cold rolling in a 3.5% sodium chloride (NaCl) solution at 90 °C.

Martensite content (%)	R_s ($\Omega \text{ cm}^2$)	Q_m ($\Omega \text{ s}^n \text{ cm}^{-2}$)	n	R_m ($\Omega \text{ cm}^2$)	C_d (F cm^{-2})	R_{ct} ($\Omega \text{ cm}^2$)
0	2.16	3.055E-5	0.7634	5.068	0.0002957	6746
0.6	1.823	7.296E-5	0.7761	3.463	0.0003169	2942
6	2.081	3.964E-5	0.7748	2.314	0.000353	3635
12	2.493	6.744E-5	0.7826	3.160	0.0003111	3643
20	2.44	6.095E-5	0.7728	3.567	0.0003387	1722

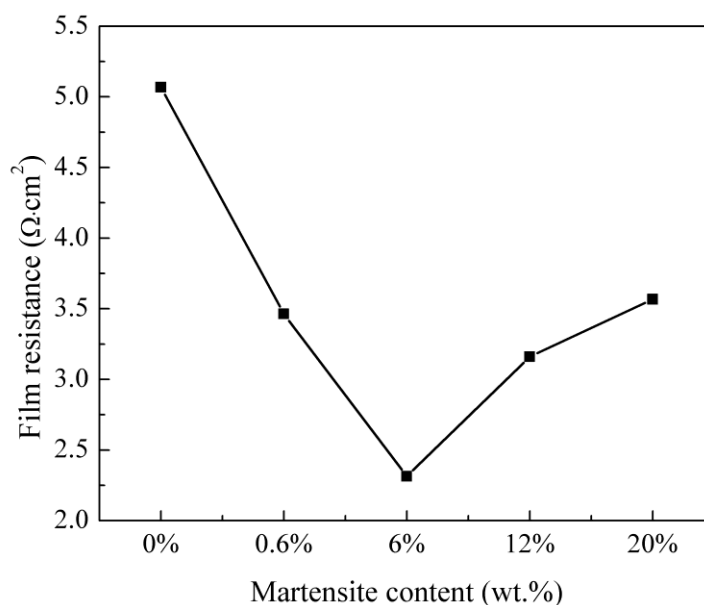


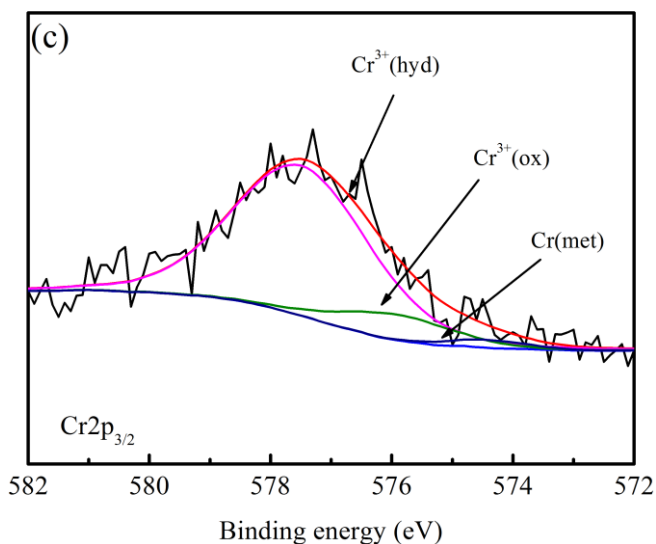
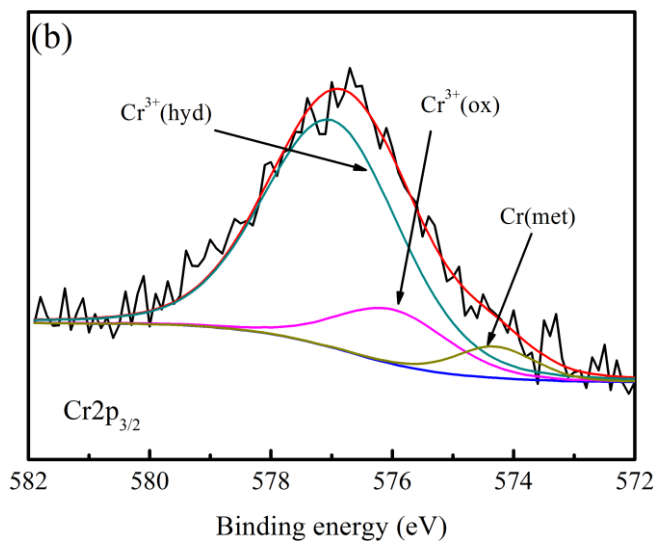
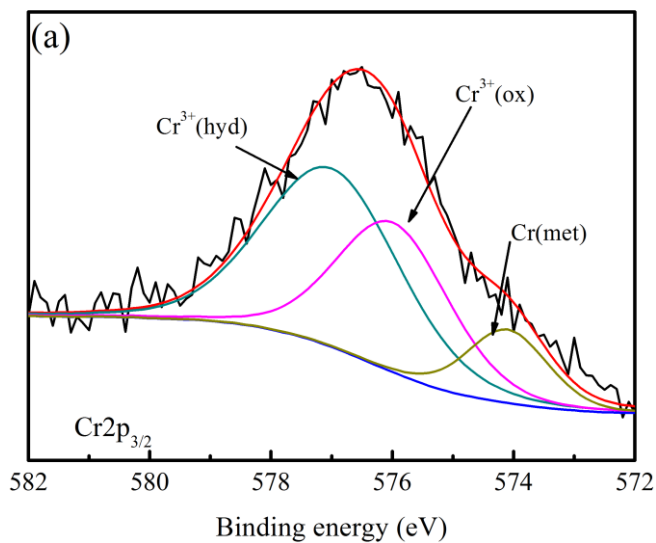
Figure 8. Film resistance (R_m) of the 304 stainless steel specimens with various martensite contents before and after cold rolling in a 3.5% sodium chloride (NaCl) solution at 90 °C.

Table 2 summarizes the electrochemical parameters fitted from the EIS data shown in Figure 6. Figure 8 shows the changes in the film resistance (R_m) of the 304 stainless steel specimens with various martensite contents before and after cold rolling. Compared to pure austenite, all the specimens containing α' -martensite had significantly lower R_m values. As the α' -martensite content increased, the R_m of the stainless steel initially decreased, reached a minimum value at an α' -martensite content of 6%, and then started to increase. The fitting results further corroborate the analysis results of the polarization curves. Notably, the passive film on the surface of the specimen with an α' -martensite content of 6% exhibited the poorest protective performance.

3.3 Changes in the composition of the passive surface film

To understand the effects of the deformation-induced martensite on the compound phases in the passive surface film, the specimens were each subjected to XPS analysis. Figure 9 and Figure 10 show the $\text{Cr}2p_{3/2}$ and $\text{Fe}2p_{3/2}$ XPS energy spectra of the 304 stainless steel specimens with various martensite

contents before and after cold rolling, respectively. The analysis results show relatively significant differences in the compound phase contents between the passive films on the surfaces of specimens with various microstructures.



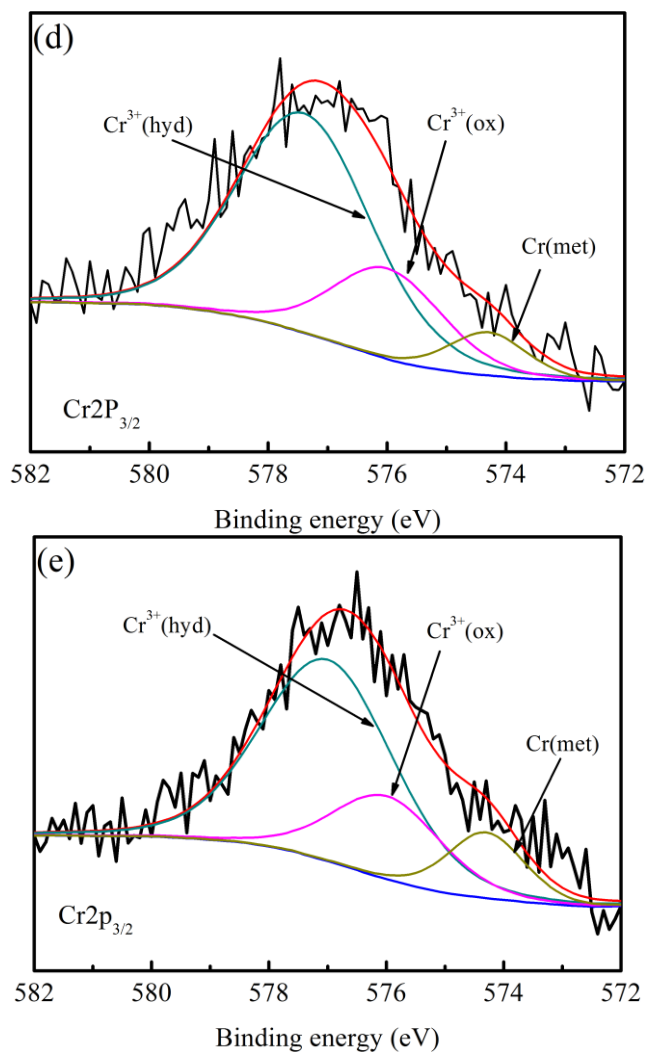
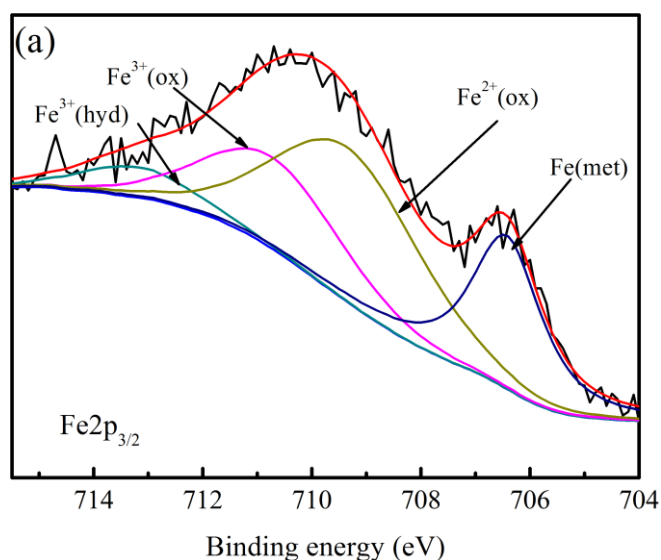
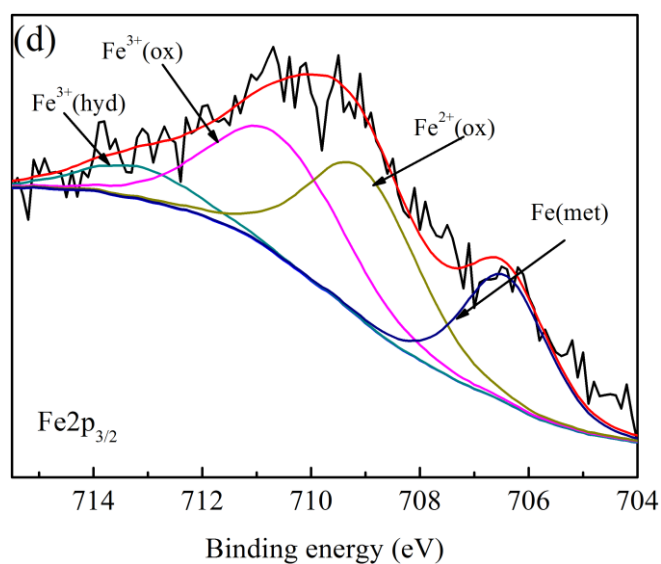
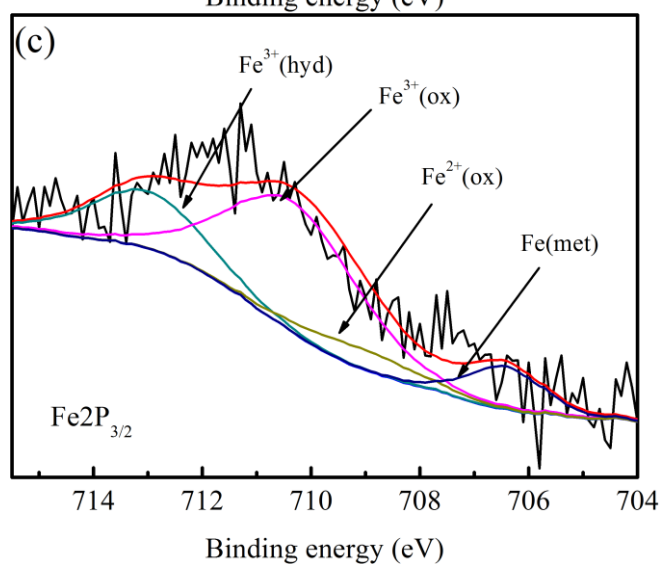
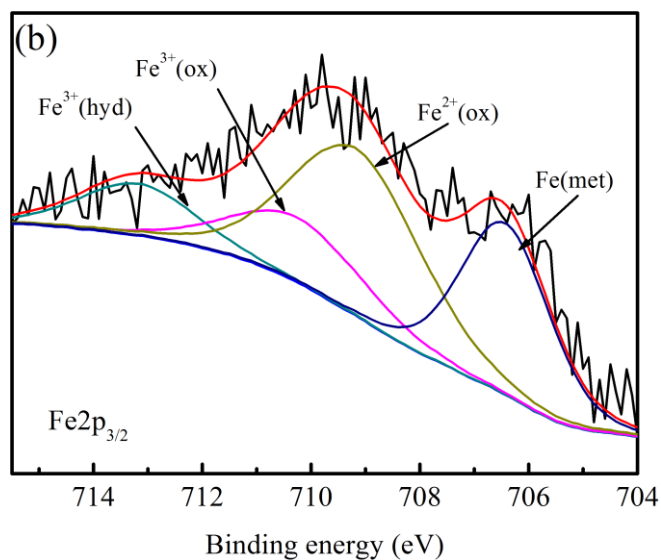


Figure 9. Cr_{2p_{3/2}} XPS energy spectra of passive films on the surfaces of the 304 stainless steel specimens with various martensite contents before and after cold rolling: (a) specimen with an α' -martensite content of 0%; (b) specimen with an α' -martensite content of 0.6%; (c) specimen with an α' -martensite content of 6%; (d) specimen with an α' -martensite content of 12% and (e) specimen with an α' -martensite content of 20%.





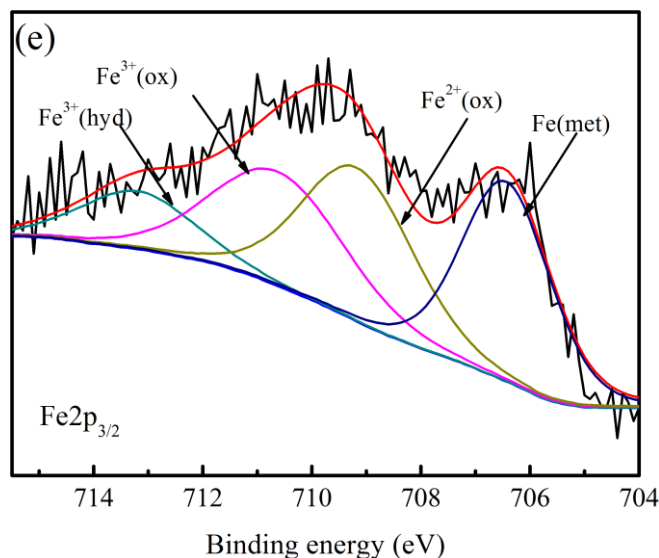


Figure 10. Fe_{2p_{3/2}} XPS energy spectra of passive films on the surfaces of the 304 stainless steel specimens with various martensite contents before and after cold rolling: (a) specimen with an α'-martensite content of 0%; (b) specimen with an α'-martensite content of 0.6%; (c) specimen with an α'-martensite content of 6%; (d) specimen with an α'-martensite content of 12% and (e) specimen with an α'-martensite content of 20%.

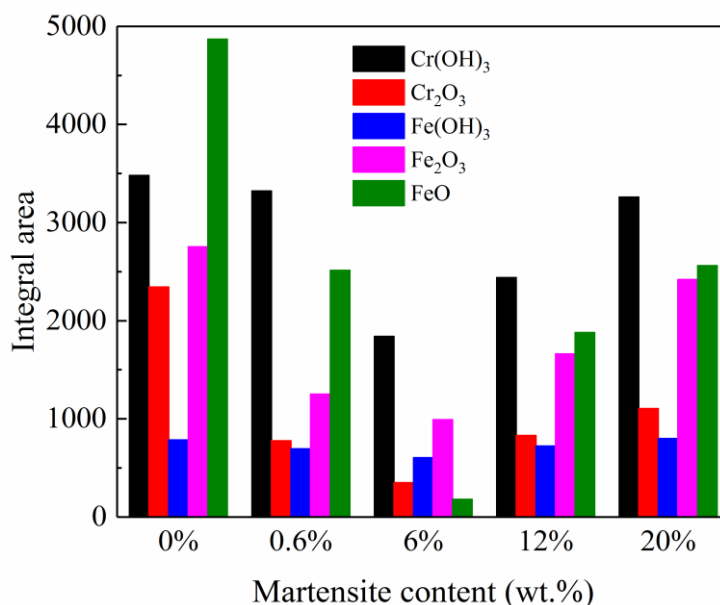


Figure 11. Compound contents of the passive films on the surfaces of the 304 stainless steel specimens with various martensite contents before and after cold rolling.

The XPS data were collected at the same time. Thus, the difference in the content of each compound phase can be determined by comparing the integrals (areas under the curves). For ease of analysis, the integral of the fitted curve (area under the fitted curve) of each compound in the passive film on the surface of the 304 stainless steel specimens with various martensite contents before and after cold rolling is presented in one diagram, as shown in Figure 11. When the α'-martensite content

was less than 6%, the Cr³⁺ (oxide), Fe²⁺ (oxide) and Fe³⁺ (oxide) contents of the passive film decreased with increasing α' -martensite content. When the α' -martensite content exceeded 6%, the contents of these three oxides in the passive film increased with increasing α' -martensite content. An inflection point can be observed in the variation curves of the contents of each of the three oxides in the passive film at an α' -martensite content of 6%. The changes in the α' -martensite content had a relatively significant impact on the contents of Cr and Fe oxides in the passive film.

4. DISCUSSION

4.1 Effects of deformation-induced martensite on surface passivation

The XRD analysis shows that a $\gamma \rightarrow \alpha$ transformation was induced when the 304 austenitic stainless steel underwent plastic deformation, when the α' (110) phase content increased relatively rapidly (Figure 3). This occurred because the deformation caused the austenitic structure to preferentially glide along the α' (110) plane[14]. It has been reported that low-strain plastic deformation can also induce a $\gamma \rightarrow \epsilon$ transformation or a $\gamma \rightarrow \epsilon \rightarrow \alpha'$ transformation. However, the characteristic peaks of ϵ -martensite are not observed in the XRD patterns because the formation mechanism of ϵ -martensite is a function of temperature and the rate of deformation[26]. The absence of ϵ -martensite in the specimens is potentially because the ϵ phase was the intermediate phase of the $\gamma \rightarrow \epsilon \rightarrow \alpha'$ transformation and was not contained in the specimens, or because the temperature and low strain rate inhibited the growth of ϵ -martensite, such that a $\gamma \rightarrow \epsilon$ transformation did not occur[14,24,26, 31,33,34].

After the solution treatment, the 304 austenitic stainless steel exhibited a uniform equiaxed austenitic structure with dislocations distributed inside the grains and no martensite content. Of the specimens with α' -martensite content of 0.6% and 6%, the specimen with an α' -martensite content of 6% was found to contain more highly deformed grains and larger structural defects than that with an α' -martensite content of 0.6%. In the specimen with an α' -martensite content of 0.6%, parallel lath martensite with the same length as the grains could be observed, and the deformation of the grains was insignificant. Compared to the specimen with an α' -martensite content of 0.6%, a greater lath martensite density was observed in the specimen with an α' -martensite content of 6%, in which crossed lath martensite and slightly deformed grains were also visible. As the α' -martensite content increased, the dislocation density in the martensite substructure also significantly increased. However, the structural changes mainly consisted of planar arrangement dislocations and stacking faults, whereas dislocation tangles were inconspicuous. Studies have found that the main modes of deformation of a face-centered cubic metal include twinning, martensite phase transformations and dislocation slips, and the deformation process is closely related to the stacking fault energy (SFE) of the material[31,33-39]. When $SFE < 18 \text{ mJ}\cdot\text{m}^{-2}$, phase transformations are the main deformation mechanism of the material. When $18 \text{ mJ}\cdot\text{m}^{-2} < SFE < 45 \text{ mJ}\cdot\text{m}^{-2}$, twinning plays a dominant role in the deformation of the material[36-39]. Stress- and strain-induced martensite phase transformations are the two main types of martensite phase transformation in Fe alloys[13]. 304 stainless steel is a low-SFE (approximately 26

mJ·m⁻²) austenitic stainless steel, and its plastic deformation structures are often planar arrangement dislocations and stacking faults at room temperature[36-39]. Thus, at this stage, the structural changes were mainly characterized by the destruction of austenite and the emergence of lath martensite in the grains. In the specimens with an α' -martensite content exceeding 6%, the grains were significantly deformed in the rolling direction and exhibited a flat shape. The higher the α' -martensite content was, the more significant the tensile deformation of the grains was. In the specimen with an α' -martensite content of 20%, the grain boundaries were indistinct, and the grains could not be easily distinguished. In addition, dislocation tangles in the structure were also found to be denser than those in other specimens. The dislocation density increased with increasing α' -martensite content, and a grid pattern of twinned crystals appeared in the deformed structure. The flow stress of a metal is directly proportional to the square root of its dislocation density[11]. This relationship explains why dislocation tangles appeared in large numbers in the specimens with α' -martensite contents of 12% and 20%. The structural changes in these two specimens were characterized by the rupture of relatively long lath martensite and an increase in the number of dislocation tangles.

The XPS analysis shows that the Cr³⁺ (oxide), Fe²⁺ (oxide) and Fe³⁺ (oxide) contents of the passive film on the surface of the stainless steel first increased and then decreased with increasing α' -martensite content (the lowest contents occurred when the α' -martensite content reached 6%). Clearly, the α' -martensite content affected the compound contents of the passive film on the surface of the stainless steel formed from passivation. The passivation capability of the matrix of a material is directly related to the microstructure. After the solution treatment, the austenitic stainless steel exhibited a relatively high surface passivation capability. When the α' -martensite content was in the range of 0–6%, the decomposition of the austenitic phase constituted the main microstructural change during the deformation of the stainless steel. The compound contents of the passive film on the surface of the stainless steel, as well as the passivation capability of the stainless steel, decreased with increasing α' -martensite content. When the α' -martensite content was in the range of 6–20%, the compound contents of the passive film on the surface of the stainless steel increased as the α' -martensite content increased, and the passivation capability of the stainless steel also increased to a certain extent. This result verifies the previous finding that it is very likely that the compounds in a passive film, as well as the thickness of a passive film, will change through deformation[17]. The occurrence of this phenomenon is likely a result of a change in the passivation mechanism of the material caused by structural changes.

4.2 Effects of deformation-induced martensite on the protective performance of the passive film

Microstructural changes in a material lead to changes in its passivation capability and directly affect the protective performance of its surface film[13,15,16,40]. As shown in the electrochemical test (polarization curve and electrochemical impedance spectroscopy measurements) results of all the specimens before and after cold rolling, the changes in the breakdown potential and the film resistance both indicated that the austenite specimen before cold rolling that was subjected to the solution treatment had the highest corrosion resistance, and the passive film contained the most oxide and

hydroxide; for the cold rolled specimens, the changes in the electrochemical properties of the stainless steel exhibited two characteristics, the protective performance of the passive film and the contents of the oxide and hydroxide decreased with increasing α' -martensite content when the α' -martensite content was less than 6%, nevertheless, the pattern observed when the α' -martensite content exceeded 6% was opposite that observed when the α' -martensite content was less than 6%, when the α' -martensite content exceeded 6%, the protective performance of the passive film and the contents of the oxide and hydroxide increased to a certain extent with increasing α' -martensite content in this study. The XPS measurements showed that the protective performance of the passive film changed in the same pattern as the Cr^{3+} (oxide) content of the passive film, which demonstrated that the electrochemical properties of the stainless steel were affected by the changes in the compound contents of its surface passive film, and this is because the dense Cr_2O_3 layer in the passive film played a major role in providing protection[41-44]. This finding is in agreement with the conclusions derived from other studies, which are supported by a number of theories[9,14,45-47]. For example, the α' -martensite in a body-centered cubic structure has a lower atomic density than the austenite in a face-centered cubic structure and undergoes volumetric expansion during the phase transformation process; as a result, a large number of protuberances are formed on the material surface[31,33-35]. Surface roughness will reduce the corrosion resistance of a material[35]. Some research has demonstrated that the conductivity of a passive film and the donor and acceptor densities in a neutral chloride solution are closely related to the thickness of the passive film and the pH of the solution[48,49]. The susceptibility of a passive film to pitting is determined by the donor density[9]. Passive films on the surfaces of martensitic steels are more sensitive to chloride ions and have significantly higher donor and acceptor densities than those on the surfaces of austenitic steels[9,33,50]. Compared to austenitic steels, passive films formed on the surfaces of martensitic steels are less stable, and ion channels can be more easily formed in these films, resulting in a reduction in their protective performance[9,51]. The changes in the α' -martensite content resulted in changes in the Cr^{3+} (oxide) content of the passive film, which in turn resulted in changes in the corrosion resistance of the passive film, however, further research is needed to determine how microstructural changes affect the passivation capability of a material and subsequently affect its electrochemical properties.

4. CONCLUSIONS

In this study, the relationships between the structural characteristics of and the composition and corrosion resistance of passive films on the surfaces of 304 stainless steel specimens with an α' -martensite content varying from 0 to 20% were examined using XRD, TEM and electrochemical methods. The conclusions derived from this study are summarized as follows:

- (1) After the solution treatment, the 304 stainless steel structure mainly consisted of a pure γ phase, and the deformation-induced martensite mainly consisted of α' -martensite.
- (2) As its α' -martensite content increased from 0 to 20%, the stainless steel underwent a number of changes: the austenite grains underwent deformation; lath martensite appeared→the lath martensite density increased→the grains were destroyed→the grains were completely destroyed; and

dislocation tangles became denser.

(3) The deformation-induced martensite had a relatively significant impact on the oxide contents of the surface passive film. When the α' -martensite content was less than 6%, the oxide content of the passive film decreased with increasing α' -martensite content. When the α' -martensite content exceeded 6%, the oxide content of the passive film increased with increasing α' -martensite content.

(4) When the α' -martensite content was less than 6%, the protective performance of the passive film decreased with increasing α' -martensite content. When the α' -martensite content exceeded 6%, the protective performance of the passive film increased to a certain extent with increasing α' -martensite content.

References

1. G. Santiago-Hurtado, M.A. Baltazar-Zamora, J. Olguin-Coca, L.D. López L, R. Galván-Martínez, A. Ríos-Juárez, C. Gaona-Tiburcio and F. Almeraya-Calderón, *Int. J. Electrochem. Sci.*, 11 (2016) 2994.
2. Y.A. Albrimi, Y.A. Addi, J. Douch, M. Hamdani and R.M. Souto, *Int. J. Electrochem. Sci.*, 11 (2016) 385.
3. C. KÖSE and R. KAÇAR, *Int. J. Electrochem. Sci.*, 11 (2016) 2762.
4. C.G. Tiburcio, F.H.E. López, P.Z. Robledo, J.A. Cabral, C.B. Durtewitz and F.A. Calderón, *Int. J. Electrochem. Sci.*, 11 (2016) 1080.
5. R.Y. Khaled, A.M. Abdel-Gaber and H.M. Holail, *Int. J. Electrochem. Sci.*, 11 (2016) 2790.
6. E.F. Pieretti and M.D. Neves, *Int. J. Electrochem. Sci.*, 11 (2016) 3532.
7. A. Samide, G.E. Iacobescu, B. Tutunaru and C. Tigae, *Int. J. Electrochem. Sci.*, 12 (2017) 2088.
8. M.C. Ramírez-López, L.A. Falcón-Franco, F.F. Curiel-López, P. Zambrano R, J.A. Cabral-Miramontes, C. Gaona-Tiburcio and F. Almeraya-Calderón, *Int. J. Electrochem. Sci.*, 12 (2017) 4928.
9. J.L. Lv and H.Y. Luo, *Appl. Surf. Sci.*, 263 (2012) 29.
10. M.D.C. Belo, M. Walls, N.E. Hakiki, J. Corset, E. Picquenard, G. Sagon and D. Noël, *Corros. Sci.*, 40 (1998) 447.
11. X. Gao, X.Q. Wu, H. Guan and E.H. Han, *J. Supercrit. Fluid.*, 42 (2007) 157.
12. J.L. Lv and H.Y. Luo, *Mater. Chem. Phys.*, 135 (2012) 973.
13. L. Hamadou, A. Kadri and N. Benbrahim, *Appl. Surf. Sci.*, 252 (2005) 1510.
14. J.L. Lv and H.Y. Luo, *Mater. Sci. Eng. A.*, 34 (2014) 484.
15. B.T. Lu, J.L. Luo and Y.C. Lu, *Electrochim. Acta.*, 53 (2008) 4122.
16. J. Sikora, E. Sikora and D.D. Macdonald, *Electrochim. Acta.*, 45 (2000) 1875.
17. S.V. Phadnis, A.K. Satpati, K.P. Muthe, J.C. Vyas and R.I. Sudaresan, *Corros. Sci.*, 45 (2003) 2467.
18. C.L. Briant and A.M. Ritter, *Scr. Metall.*, 13 (1979) 177.
19. C.L. Briant and A.M. Ritter, *Metall. Trans. A.*, 11 (1980) 2009.
20. A.S. Hamdy, E.E. Shenawy and T.E. Bitar, *Mater. Lett.*, 61 (2007) 2827.
21. U.K. Mudali, P. Shankar, S. Ningshen, R.K. Dayal, H.S. Khatak and B. Raj, *Corros. Sci.*, 44 (2002) 2183.
22. Z.S. Smialowska, *Corrosion*, 27 (1971) 223.
23. P. Forchhammer and H.J. Engell, *Mater. Corros.*, 20 (1969) 1.
24. K. Guan, X.H. Zhang, X.D. Gu, L.Z. Cai, H. Xu and Z.W. Wang, *Eng. Fail. Anal.*, 12 (2005) 387.
25. I. Nicic and D.D. Macdonald, *J. Nucl. Mater.*, 379 (2008) 54.

26. K. Datta, R. Delhez, P.M. Bronsveld, J. Beyer, H.J. M. Geijselaers and J. Post, *Acta. Mater.*, 57 (2009) 3321.
27. B. Stellwag, *Corros. Sci.*, 40 (1998) 337.
28. Y.L. Sandler, *Corrosion*, 35 (1979) 205.
29. T. Miyazawa, S. Uchida, T. Satoh, Y. Morishima, T. Hirose, Y. Satoh, K. Iinuma, Y. Wada, H. Hosokawa and N. Usui, *J. Nucl. Sci. Technol.*, 42 (2005) 233.
30. M.C. Sun, X.Q. Wu, Z.E. Zhang and E.H. Han, *Corros. Sci.*, 51 (2009) 1069.
31. H.N. Han, C.G. Lee, C.S. Oh, T.H. Lee and S.J. Kim, *Acta. Mater.*, 52 (2004) 5203.
32. C.M. Rangel, T.M. Silva and M.D.C. Belo, *Electrochim. Acta.*, 50 (2005) 5076.
33. G.B. Olson and M. Cohen, *J. Less-Common. Met.*, 28 (1972) 107.
34. M.R.D. Rocha and C.A.S.D. Oliveira, *Mater. Sci. Eng. A.*, 517 (2009) 281.
35. E. Nagy, V. Mertinger, F. Tranta and J. Sólyom, *Mater. Sci. Eng. A.*, 378 (2004) 308.
36. G.B. Olson and M. Cohen, *Metall. Trans. A.*, 7 (1976) 1897.
37. R.L. Nolder and G. Thomas, *Acta Metall.*, 11 (1963) 994.
38. M.A. Meyers, U.R. Andrade and A.H. Chokshi, *Metall. Mater. Trans. A.*, 25 (1995) 2681.
39. H.J. Lai, and C.M. Wan, *Scr. Metall.*, 23 (1989) 179.
40. H. Sun, X.Q. Wu, E.H. Han and Y.Z. Wei, *Corros. Sci.*, 59 (2012) 334.
41. A.M.P. Simoes, M.G.S. Ferreira, G. Lorang and M.D.C. Belo, *Electrochim. Acta.*, 36 (1991) 315.
42. G.M. Bulman and A.C. Tseung, *Corros. Sci.*, 12 (1972) 415.
43. S. Maximovitch, *Electrochim. Acta.*, 41 (1996) 2761.
44. N.E. Hakiki, S. Boudin, B. Rondot and M.D.C. Belo, *Corros. Sci.*, 37 (1995) 1809.
45. D.D. MacDonald and A. Sun, *Electrochim. Acta.*, 51 (2006) 1767.
46. V.S. Battaglia and J. Newman, *J. Electrochem. Soc.*, 142 (1995) 1423.
47. M.K. Kumar, K. Gaonkar, S. Ghosh, V. Kain, M. Bojinov and T. Saario, *J. Nucl. Mater.*, 401 (2010) 46.
48. C.M. Abreu, M.J. Cristobal, R. Losada, X.R. Novoa and G. Pena, *J. Electroanal. Chem.*, 572 (2004) 335.
49. R. Babic and M. Metikos-Hukovic, *J. Electroanal. Chem.*, 358 (1993) 143.
50. J.B. Lee and S.I. Yoon, *Mater. Chem. Phys.*, 122 (2010) 194.
51. M. Metikos-Hukovic, R. Babic, Z. Grubac, Z. Petrovic and N. Lajci, *Corros. Sci.*, 53 (2011) 2176.

© 2018 The Authors. Published by ESG (www.electrochemsci.org). This article is an open access article distributed under the terms and conditions of the Creative Commons Attribution license (<http://creativecommons.org/licenses/by/4.0/>).